Nuclear Instruments and Methods in Physics Research A 639 (2011) 158–161

Contents lists available at ScienceDirect

Nuclear Instruments and Methods in Physics Research A

journal homepage: www.elsevier.com/locate/nima

Simulation of gain and timing resolution in saturated pores

Valentin Ivanov [a,*], Zeke Insepov [b], Sergey Antipov [b]

[a] Muons, Incorporated, 552 N. Batavia Avenue, Batavia, IL 60610, USA
[b] Argonne National Laboratory, 9700 S. Cass Avenue, Argonne, IL 60439, USA

ARTICLE INFO

Available online 13 November 2010

Keywords:
Micro-channel plate
Secondary emission
Saturation
Gain
Timing resolution

ABSTRACT

Micro-channel plate (MCP) amplifiers are commonly used in detectors of fast time signals with picosecond resolution. The main parameters of the MCP amplifier, such as the gain factor and time resolution are strongly dependent on the work regime of the device. The saturation effects occur with a high-level input signal. In our paper these effects are studied numerically for large-area fast photo-detectors. It is shown that the saturation effect for short pulses can be reduced by introducing a thin, resistive layer between the bulk material and the emissive coating. A set of 2D and 3D numerical tools (MCP simulator, Monte Carlo simulator) was developed to simulate photo, secondary emission, fringe fields, and saturation phenomena in MCP amplifiers. The gain and time resolution dependencies on the pore size and voltage were studied numerically. The results are compared with the simulations of other authors and available experimental data.

Published by Elsevier B.V.

1. Introduction

Many measurements in particle and accelerator physics are limited by the time resolution with which individual particles can be detected. These measurements include particle identification by time of flight in major experiments such as CDF at Fermilab and Atlas and CMS at the Large Hadron Collider, as well as measurement of longitudinal variables in accelerator physics experiments.

A large-area photo-detector consists of the photo-cathode accepting photons from an external source, a micro-channel plate (MCP), a segmented anode, and accelerating gaps between them (Fig. 1). The MCP produces cascades of secondary electrons to be detected by the anode circuit.

MCP amplifiers have been studied numerically by many authors in Refs. [1–3].

2. Numerical model of saturation effect

As was shown by Guest [1], the longitudinal current distribution in the pore has an exponential dependence. This means that a huge number of secondary electrons are extracted from the end of the pore for short input pulse and high gain, and a positive charge is induced on the pore surface thereby suppressing further secondary emission. The current from an external source cannot compensate for the induced charge immediately because of the finite resistance of the secondary emitter material. The saturation effect can be mitigated by two approaches. The first is to make a double-layer cover on the pore surface: a high-conductivity layer below and a high-emission layer on top. The second approach can be realized in a MCP chevron pair or Z-stack by varying the intermediate gap. Here the secondary electron beam from the first plate is redistributed to the neighbor pores of the second plate. This approach reduces the current in an individual channel, and reduces the saturation effect. We studied both approaches numerically.

Different models of the saturation effect in an MCP have been suggested in Refs. [4–6]. All of them include some coefficients to fit the gain vs. voltage dependence to the experimental data. Berkin et al. give an analytical solution for the pulse [7] and DC [8] work regimes, which include the easily measured parameters only for the electric field

$$E_z(z,t) = E_{0z} h_E(z,t), \tag{1}$$

and gain

$$M(z,t) = M_0 \frac{h_E(z,t)}{1-[h_E(z,t_p)-1]\exp\left((t_p-T)/\tau\right)}. \tag{2}$$

The shape function is given by the following formulas:

$$h_E(z,t) = \frac{\ln(M_0)}{[\ln(M_0)-\ln(1+C(t))-\ln(1+C(t)M_0)][1+C(t)e^{\alpha z}]},$$

$$c(t) = \frac{I_0}{I_R}(1-e^{-t/\tau}), \tag{3}$$

here E_{0z}, M_0 are the electric field and gain for the non-saturated mode, respectively; T, t_p are the pulse period and pulse length, respectively; τ is a charge relaxation time (CRT); I_0, I_R are the input

* Corresponding author. Tel.: +1 408 568 1483.
E-mail address: vivanov@fnal.gov (V. Ivanov).

0168-9002/$ - see front matter Published by Elsevier B.V.
doi:10.1016/j.nima.2010.10.052

current and resistance current, respectively; α is the increment of the emission current in non-saturated pore $I(z)=I_0\exp(\alpha z)$, z is the axial coordinate; t is the time.

Figs. 2 and 3 show the results of our simulations for 20 μm pores of 1.2 mm length. One can see that the saturation effects are negligible for $I_0 < 10^{-15}$ A.

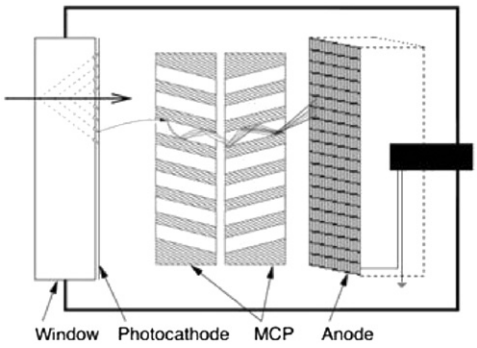

Fig. 1. MCP photo-detector.

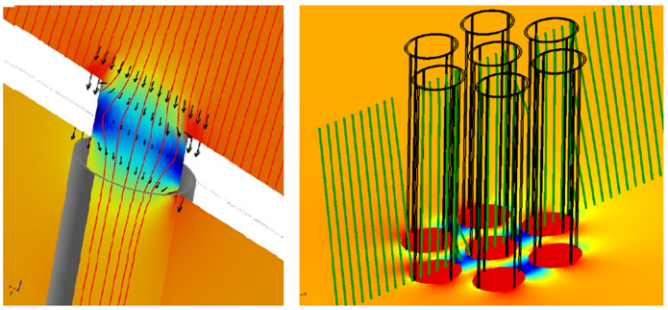

Fig. 4. The lines of electric field in the pores (left) and between them (right).

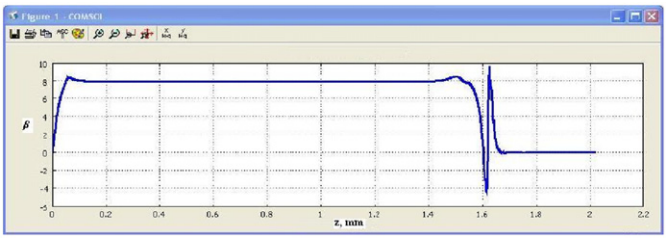

Fig. 5. Edge effect for the electric field.

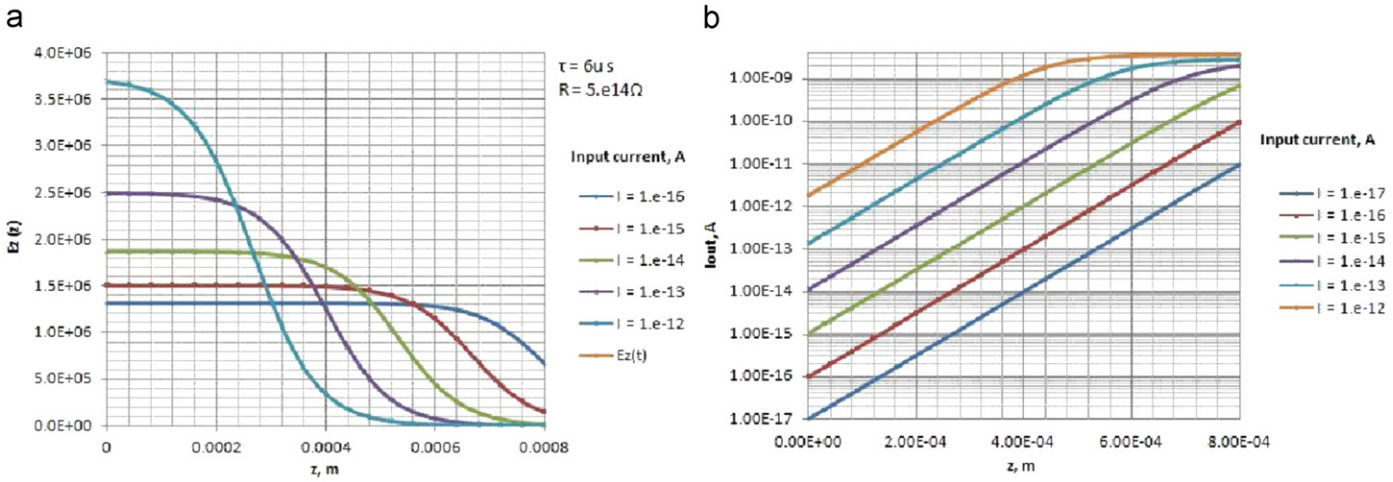

Fig. 2. (a) Field distribution in the channel for different input current; (b) output current distribution vs. input currents.

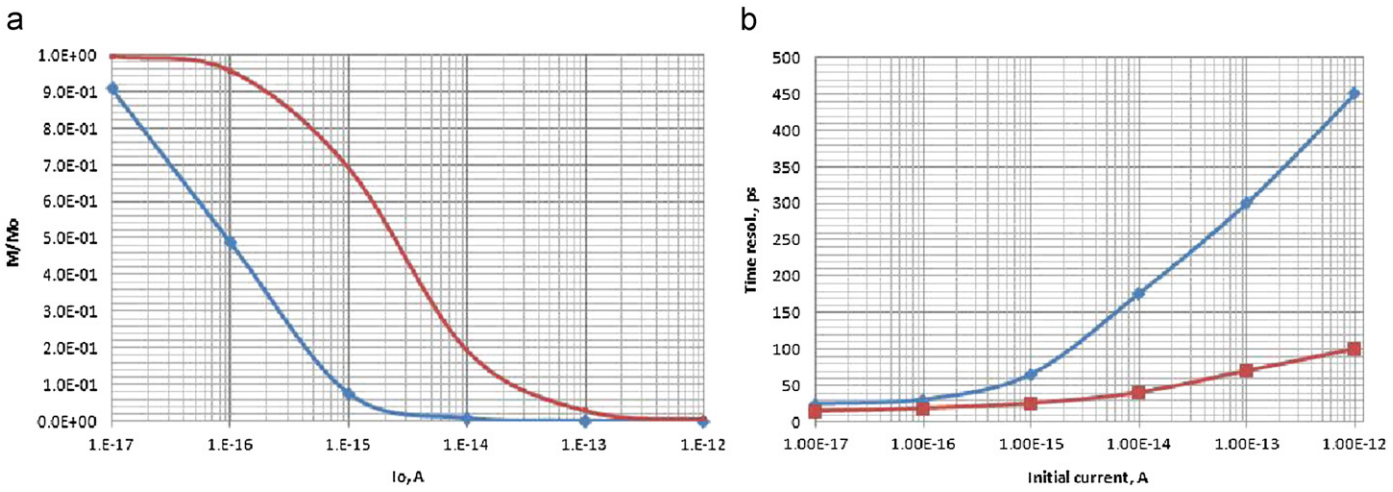

Fig. 3. (a) Gain vs. input current for $\tau=1$ ms (diamonds) and $\tau=1$ μs (squares); (b) timing resolution vs. input current.

3. Fringe field simulation in 3D

We have simulated the electric field inside the pores of chevron-type MCPs using the multi-physics COMSOL software and verified this study by an analytical solution. The simulations show that in a highly-conductive environment, the electric field in the pore is directed axially inside the pore, having a gradual turn from the value in the resistive layer near the surface. In a simulation we assume that the relaxation time ε/σ is small for a thin resistive layer comprising a mixture 30% Al_2O_3 and 70% ZnO.

Fig. 4 shows the lines of electric field in 1 and 7 pores with bias angle of 8°.

Fig. 5 demonstrates the edge effect at the end of pore—the angle $\beta = a\tan(E_x/E_z)\times 100/\pi$ vs. z-coordinate of the pore.

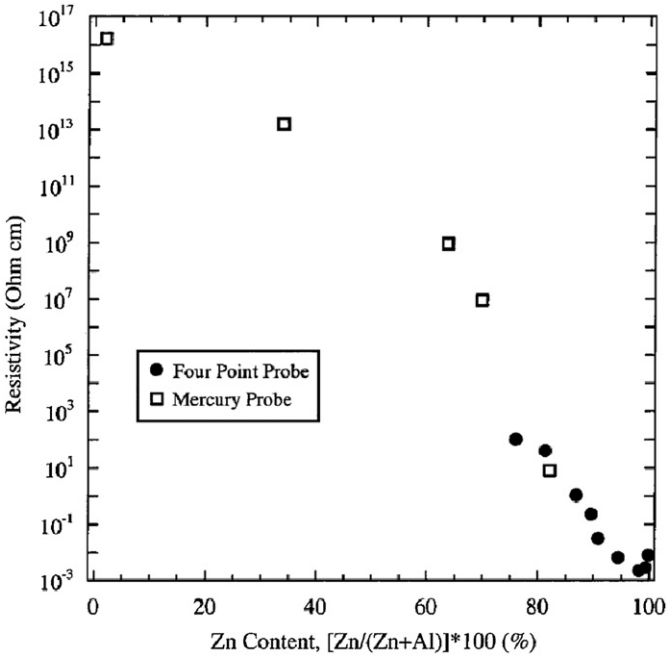

Fig. 6. Measured resistivity of ZnO/Al_2O_3 alloy films.

4. Charge relaxation time computation

ZnO/Al_2O_3 alloy films were prepared using atomic layer deposition (ALD) techniques. By adjusting the ALD pulse sequence, the ZnO/Al_2O_3 alloy film composition was varied from 0% to 100% ZnO [10]. Fig. 6 shows the resistivity of ZnO/Al_2O_3 alloy films used in this work. The material constants and physical properties of these alloy films, such as surface roughness, resistivity, dielectric constants, and film thickness were selected so that these materials could be used as resistive and emissive layers in large-area photo-detecting MCPs, as compared with conventional glass substrates. Charge relaxation and gain depletion mechanisms, effects of a strong electric field, and geometry parameters of the coating for large-area, fast photo-detectors were analyzed and discussed in Ref. [11].

A new ambipolar solid state plasma drift-diffusion model of the charge relaxation in such materials as ZnO/Al_2O_3 in various combination of the content was proposed that included generation of electrons and holes via impact ionization due to acceleration in a strong electric field [12]. Some of the equations of this model are given below [13–16]:

$$\vec{J}_e = eD_e\nabla N_e + e\mu_e N_e\vec{E},$$

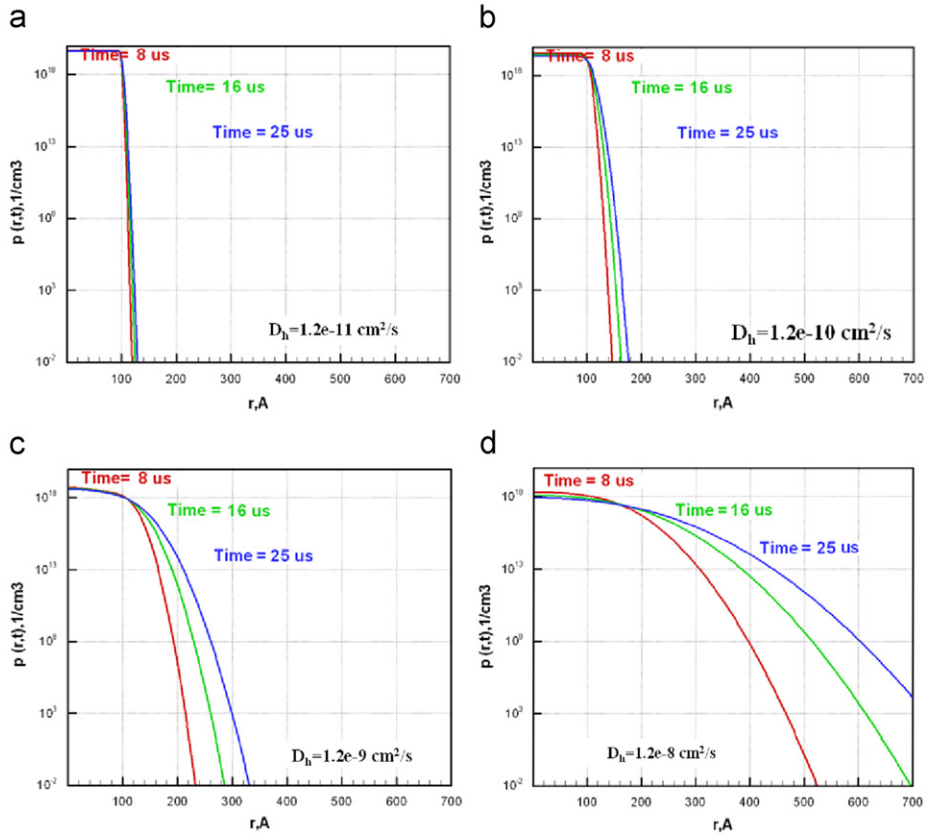

Fig. 7. Results of our calculation with the drift-diffusion model in spherical geometry, with the diffusion coefficients shown in the plots: (a) 1.2×10^{-11}, (b) 1.2×10^{-10}, (c) 1.2×10^{-9}, and (d) 1.2×10^{-8} cm^2/s.

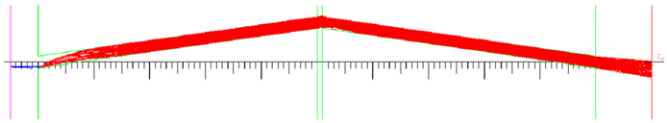

Fig. 8. Small gap: gain $M=1.2\times10^6$ for $\tau=1$ μs and $M=1.5\times10^5$ for $\tau=1$ ms.

$$\vec{J}_h = -eD_h\nabla N_h + e\mu_h N_h\vec{E},$$
$$div\ \vec{E} = \frac{\rho}{\varepsilon\varepsilon_0},\ \rho = N_h - N_e,$$
$$\frac{\partial N_e}{\partial t} = \frac{1}{q}\nabla J_e = D_e\Delta N_e + eN_e\mu_e/\varepsilon\varepsilon_0(N_h - N_e) + G_{ii},$$
$$\frac{\partial N_h}{\partial t} = -\frac{1}{q}\nabla J_h = D_h\Delta N_h - eN_h\mu_h/\varepsilon\varepsilon_0(N_h - N_e),$$
$$\mu_{e,h} = \sigma_{e,h}/eN_{e,h},\quad D_{e,h} = \mu_{e,h}k_BT/e.$$

here e is the elemental charge amount ($e>0$), $D_{e,h}$ are the diffusion coefficients, and $\mu_{e,h}$ are the mobility of electrons and holes at temperature T created by electron impacts and ionization in the space charge field, G_{ii}. The Einstein relationship between the diffusion coefficients and the mobility allows use of the electric-field-dependent diffusion coefficients; $N_{e,h}$ are the corresponding carrier densities; and $J_{e,h}$ are the fluxes of carriers.

The following conductivity of AZO film with 20% Al was used: $\mu=10^7$ (Ω cm). The diffusion coefficients of amorphous alumina are unknown. Therefore, we used the diffusion coefficients of alumina via alumina carrier mobility that are given for some limited mixture content in Ref. [17]. Assuming linear dependence between conductivity and mobility, the mobility of a mixture Al_2O_3+ZnO was extrapolated from low to high Al content.

The calculated results (Fig. 7) were compared with the results of a simple Maxwell relaxation time model and with the circuit charge relaxation model developed for the MCP device [18]. A pump-probe experiment is in principle capable of measuring the charge relaxation time, and to clearly demonstrate gain depletion [19].

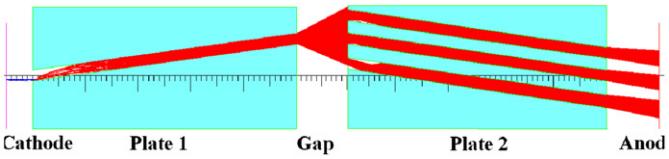

Fig. 9. Large gap: electrons distributed to 7 pores of the second plate. Gain $M=3.4\times10^6$ for $\tau=1$ μs and $M=1.13\times10^6$ for $\tau=1$ ms.

5. Mitigation of saturation effect

Monte Carlo algorithms are commonly used in simulation of MCP amplifiers [9]. The effect of inter-plate gap variation was studied numerically using full 3D Monte Carlo Simulator "MCS" code. Fig. 8 shows that most of the beam from the first plate is accepted by one pore of the second plate for a gap size of 15 μm. The same initial beam is redistributed for 7 pores of a hexagonal structure in a second MCP for a gap of 100 μm (Fig. 9), which substantially reduces the saturation effect.

References

[1] A.J. Guest, Acta Electron. 14 (1)(1971) 79.
[2] A.M. Tutikov, et al., Sov. J. Opt. Technol. 50 (7)(1991) 392.
[3] A.S. Tremsin, et al., Nucl. Instr. and Meth. A 379 (1996) 139.
[4] P.M. Shikhalev, Nucl. Instr. and Meth. A 420 (1999) 202.
[5] G.J. Price, G.W. Fraser, Nucl. Instr. and Meth A 474 (2001) 188.
[6] G.W. Fraser, et al., IEEE Trans. Nucl. Sci. NS-30 (1)(1983) 455.
[7] A.B. Berkin, V.V. Vasil'ev, Zh. Tekn. Fiz. 78 (2)(2008) 127.
[8] A.B. Berkin, V.V. Vasil'ev, Zh. Tekn. Fiz. 78 (2)(2008) 130.
[9] E. Gatti, et al., IEEE Trans. Nucl. Sci. NS-30 (1)(1983) 461.
[10] J.W. Elam, et al., J. Electrochem. Soc. 150 (6)(2003) G339.
[11] A.K. Jonscher, Principles of Semiconductor Device Operations, Wiley, 1960.
[12] A.G. Chynoweth, J. Appl. Phys. 31 (1960) 1161.
[13] A.H. Marshak, Proc. IEEE 72 (1984) 148.
[14] R.Van Overstraeten, Solid State Electron. 13 (1970) 583.
[15] L.M. Biberman, Proc. IEEE 59 (1972) 555.
[16] Z. Insepov, et al., Phys. Rev. A 77 (2008) 062901.
[17] F. Ruske, et al., J. Appl. Phys. 107 (2010) 013708.
[18] A.B. Berkin, V.V. Vasil'yev, Tech. Phys. Lett. 33 (2007) 664.
[19] O.L. Landen, et al., Proc. SPIE 2002 (1993) 2.